JOURNAL OF MAGNETIC RESONANCE IMAGING 35:572-581 (2012)

Original Research

Modulatory Effects of Acupuncture on Resting-State Networks: A Functional MRI Study Combining Independent Component Analysis and Multivariate Granger Causality Analysis

Chongguang Zhong, PhD,[1] Lijun Bai, PhD,[1] Ruwei Dai, PhD,[1] Ting Xue, PhD,[2] Hu Wang, PhD,[1] Yuanyuan Feng, PhD,[1] Zhenyu Liu, PhD,[1] Youbo You, PhD,[1] Shangjie Chen, PhD,[3] and Jie Tian, PhD[1,2]*

Purpose: To investigate acupuncture specificity by exploring causal relationships of brain networks following acupuncture at GB40 (Qiuxu), with the acupoint KI3 (Taixi) as a control (belonging to the same nerve segment but different meridians).

Materials and Methods: Needling at acupoints GB40 and KI3 was performed in 12 subjects separately. The specific coherent patterns, resting-state networks (RSNs), were retrieved by independent component analysis (ICA) from functional magnetic resonance imaging (fMRI) data of resting state and post-acupuncture resting states, respectively. Then multivariate Granger causality analysis (mGCA) was applied to evaluate the effective connectivity within and among the detected RSNs—default model, memory, executive, auditory, and motor brain networks.

Results: Following acupuncture at GB40, the strength of causal connectivity between the superior temporal gyrus (STG) and anterior insula was enhanced, while the connection strength between the STG and postcentral gyrus increased following acupuncture at KI3. Additionally, the causal influences within the auditory network increased following acupuncture at GB40, in comparison with the executive network following acupuncture at KI3.

Conclusion: The current study demonstrates that acupuncture at different acupoints could exert different modulatory effects on RSNs. Our findings may help to understand the neurophysiological mechanisms underlying acupuncture specificity.

Key Words: acupuncture specificity; resting state networks; multivariate Granger causality analysis; ICA; fMRI
J. Magn. Reson. Imaging 2012;35:572–581.

ACUPUNCTURE ORIGINATED IN CHINA over two millennia ago and is emerging as an important modality of alternative and complementary medicine in the Western world (1). Unfortunately, the neural mechanisms underlying the efficacy of acupuncture are not well understood and controversy still remains. As one of modern in vivo neuroimaging techniques, functional magnetic resonance imaging (fMRI) provides an effective tool to safely monitor brain activity evoked by acupuncture.

Scientific evidence regarding the specific modulatory effect of acupuncture splits into two sides. Several investigations report that acupuncture stimulation at some "vision-related" acupoints can selectively evoke neural responses in the visual cortices, but such neural activities do not emerge after stimulation at a nearby non-acupoint (2,3). However, one recent study shows no significant difference of fMRI signal changes in occipital cortex among acupuncture stimulation at vision-related acupoints (UB60 and GB37) and a non-acupoint (4). In another study, Wesolowski et al (5) observed no significant activations in primary auditory cortex during stimulation of the hearing-related acupoint GB43 or a sham point. These two prior studies do not support the specificity of function-specific acupoints in comparison with another acupoint or a non-acupoint as control conditions. Despite stimulation at different acupoints, acupuncture may elicit overlapped spatial distribution of

[1]Medical Image Processing Group, Institute of Automation, Chinese Academy of Sciences, Beijing, China.
[2]Life Sciences Research Center, School of Life Sciences and Technology, Xidian University, Xi'an, China.
[3]Baoan Hospital, Southern Medical University, Shenzhen, China.

Contract grant sponsor: Knowledge Innovation Program of the Chinese Academy of Sciences; Contract grant number: KGCX2-YW-129; Contract grant sponsor: Project for the National Key Basic Research and Development Program (973); Contract grant number: 2011CB707700; Contract grant sponsor: National Natural Science Foundation of China; Contract grant numbers: 30873462, 30970774, 60901064, 81071137, 81071217, 81173354; Contract grant sponsor: Natural Science Foundation of Guangdong Province; Contract grant number: 10451810101005862.

C.Z. and L.B. contributed equally to this work.

*Address reprint requests to: J.T., Institute of Automation, Chinese Academy of Sciences, Zhong Guancun East Rd. No. 95, Beijing 100190, China. E-mail: tian@ieee.org

Received February 17, 2011; Accepted October 11, 2011.
DOI 10.1002/jmri.22887
View this article online at wileyonlinelibrary.com.

neural responses in the limbic-paralimbic-neocortical brain networks (6). Therefore, previous fMRI studies on acupuncture mainly focus on spatial distributions of increased and decreased activities of brain regions during needling manipulations (2–6). We speculated that the extant controversy of acupuncture specificity may be attributed to methodological problems.

On the whole, most previous fMRI studies that deny or evade the acupuncture specificity have generally adopted the blocked-designed model-based analysis (4,6–8). The estimates of the blood oxygenation level-dependent (BOLD) response derived from the model-based analysis (general linear model [GLM]) are completely limited by the design of the experimental paradigm and whether the stimuli can be turned on and off repeatedly (9). However, both abundant clinical reports and the Traditional Chinese Medicine theory suggest that the analgesic effects of acupuncture may last a long period even after the needling process is terminated (10,11). As one of the specific cases, psychophysical analysis from Price et al (12) demonstrates that the analgesic effects of acupuncture may actually peak long beyond the needling session. Considering the sustained effects of acupuncture, the temporal profile of BOLD responses to acupuncture may violate the "on-off" assumptions of blocked-designed GLM estimates. The effects of the elevated activity during resting state may reduce or eliminate the activity during acupuncture stimulation conditions or even reverse the sign of brain activation using conventional GLM analysis (9).

The sustained effects of acupuncture have been widely applied to clinical treatment; thus, we assumed that the relatively functional specificity of acupoints may evolve as a function of time. Some studies have already paid attention to the sustained effects of acupuncture (9,13–16), and explored its impact on the resting-state networks (RSNs) (17–19). Extensive signal attenuations evoked by acupuncture are observed in the core areas of the "default mode" network (DMN) (17). Additionally, increased DMN connectivity with pain, affective, and memory-related brain regions, and increased sensorimotor network connectivity with pain-related regions, have been observed following verum acupuncture, rather than the sham control (17). Bai et al (19) have suggested that acupuncture may not only enhance the dichotomy of the anticorrelated RSNs, but also modulate the intrinsic coherences of the wide interoceptive-autonomic brain networks, including the paralimbic regions and brainstem nuclei. Therefore, we assumed that acupuncture probably involved interactions of multiple brain networks. Our study focused on the relatively functional specificity of different acupoints via analyzing the poststimulus RSNs modulated by acupuncture.

In terms of the well-identified physical effects of acupuncture needling and its purported clinical efficacy, we presume that acupuncture acts in maintaining a homeostatic balance of the internal state within and across multiple brain systems (10,11). Previous studies have explored the modulatory effects of acupuncture on multiple RSNs with standard functional connectivity analysis, which investigated undirected relations between different brain regions (17–19). However, little is known about the causal interactions within and among these RSNs modulated by acupuncture. In the present study we combined independent component analysis (ICA) and multivariate Granger causality analysis (mGCA) to explore causal relationships of the poststimulus resting brain networks modulated by acupuncture at GB40 (Qiuxu), with a different meridian acupoint KI3 (Taixi) as a control condition. The data-driven method ICA can spatially isolate the spatial patterns of function-related neural networks from the spatial patterns of activity related to artifacts, such as subtle movements, machine noise, and cardiac and respiratory pulsations (20–22). The RSNs detected from ICA have also been proven to be highly reproducible and stable across subjects and sessions (21). The RSNs comprise the DMN, memory, executive, auditory, and motor networks. The DMN comprises the inferior temporal gyrus, anterior cingulate cortex, and posterior cingulate cortex/precuneus. The memory network includes the superior parietal lobule, frontopolar area/prefrontal cortex, and middle temporal gyrus. The executive network contains the dorsolateral prefrontal cortex and medial frontal gyrus. The auditory network embraces the superior temporal gyrus and anterior insula. The motor network contains the postcentral gyrus and precentral gyrus (21). The mGCA was then applied to evaluate the effective connectivity between these brain regions, as it can detect direct causal interactions within and among RSNs by computing directed transfer function (DTF) from a multivariate autoregressive (MVAR) model (23). By applying ICA and mGCA to explore modulatory effects of acupuncture on RSNs, we may provide a new clue to explore the neurophysiological mechanisms underlying acupuncture specificity.

In this study we combined ICA and mGCA to investigate the causal interactions within and among brain networks during the poststimulus resting state following acupuncture at GB40, with KI3 as a control. We chose the acupoint KI3 as a control because it is used to obtain similar physiologic effects from a functionally irrelevant acupoint, since it is innervated by the same spinal nerve as GB40, but belongs to different meridians. If significantly different modulatory effects on resting-state brain networks are observed during the poststimulus resting states following acupuncture at GB40 and KI3, then it stands to reason that different acupoints may bear some relative specificity. We attempted to explore the relative modulatory effects underlying acupuncture at different acupoints by examining both the directions and strengths of causal interactions within and among brain networks during the poststimulus resting states. By comparing the effective connectivity patterns of the resting state and post-acupuncture resting states, we expected to provide additional evidence to support the relative function-oriented specificity of acupuncture effects.

MATERIALS AND METHODS

Subjects

Twelve healthy Chinese right-handed volunteers (nine males, age 23.5 ± 1.2 years) were recruited from a

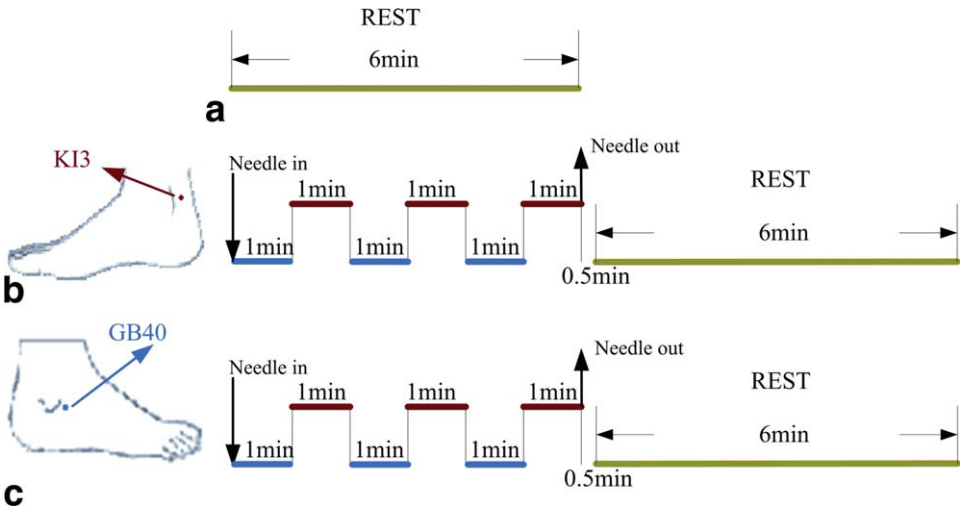

Figure 1. Experimental paradigm. **a**: A 6-minute resting state. **b**: Acupuncture stimulation was performed at acupoint KI3 on the right leg (Taixi, arrow pointing to red dot). **c**: Needling was performed at acupoint GB40 on the right leg (Qiuxu, arrow pointing to blue dot). The red line refers to epoch with needle administration, and the blue line represents no acupuncture manipulation, while the long green line indicates a 6-minute resting state and 6-minute post-acupuncture resting states. In this study, the three 6-minute rest epochs were employed, while the rest were used for further analysis. [Color figure can be viewed in the online issue, which is available at wileyonlinelibrary.com.]

homogeneous group in order to reduce intersubject differences. None of them had experienced neurological or psychiatric disorders. All of them were free of any intake of prescription medications within the last month, as well as any contraindications for exposure to a high magnetic field. All subjects were acupuncture-naïve and gave written informed consent as approved by the local Ethics Committee. All experiments were in accord with the Declaration of Helsinki.

Experimental Paradigm

All subjects first underwent a resting state scan, then half of them experienced a scan of poststimulus resting state at GB40. To mitigate any potential long-lasting effects following the acupuncture intervention, another scan of post-acupuncture resting state at KI3 was performed 7 days later. The other half of the subjects first received acupuncture treatment at KI3, then GB40 after 7 days. The acupoint GB40 on the right leg is located in a depression at the anteroinferior side of lateral malleolus and lateral to the long extensor muscle of toes (arrow pointing to blue dot in Fig. 1), while KI3 on the right leg is located in a depression between the medial malleolus and heel tendon (arrow pointing to red dot). Figure 1 shows an ON/OFF blocked-designed experimental paradigm during the fMRI scan. The three stimulation epochs were separated by two intervals of 1 minute without acupuncture stimuli. Then another 6-minute poststimulus resting scan was performed after removing the needle. A sterile disposable stainless steel acupuncture needle (0.2 mm in diameter and 40 mm in length) was used to deliver acupuncture stimulation. The needle was rotated manually clockwise and counterclockwise for 1 minute at a rate of 60 times per minute by a balanced "tonifying and reducing" technique during the experiment (7). Due to the anatomical differences of different acupoints, the needling depth of GB40 was 2.0–2.5 cm, while it was 2.5–3.0 cm for KI3. The precise locations of needling, the presumed acupuncture effects, and the stimulation paradigm were not divulged to the subjects. The procedure was performed by the same experienced and licensed acupuncturist on all subjects.

During the experiment, all subjects were instructed to keep their eyes closed and remain relaxed without engaging in any mental tasks. At the end of each scanning, the subjects were asked to quantify throbbing, aching, soreness, heaviness, fullness, warmth, coolness, numbness, tingling, dull or sharp pain, and any other sensations they experienced during the stimulus (8). The sensation rates ranged from 0 to 10 (0 = no sensation, 1–3 = mild, 4–6 = moderate, 7–8 = strong, 9 = severe, and 10 = unbearable sensation).

Data Acquisition and Analysis

All MRI data were acquired on a 1.5 T ACS-NT15 Philips scanner (Best, Netherlands) equipped with a standard head coil. Head movements were prevented by a custom-built head holder. The images were parallel to the AC-PC line and covered the whole brain. Thirty axial slices were obtained using a T2*-weighted single-shot, gradient-recalled echo planar imaging sequence (field of view [FOV] = 230 × 230 mm, matrix = 64 × 64, thickness = 5 mm, TR = 4000 msec, TE = 50 msec, flip angle = 90°). After the functional run, high-resolution structural information on each subject was also acquired using 3D MRI sequences with a voxel size of 1 mm^3 for anatomical localization (TR = 2510 msec, TE = 15 msec, matrix = 384 × 512, FOV = 230 × 230 mm, flip angle = 30°, thickness = 5 mm).

The first five volumes were discarded for eliminating nonequilibrium effects of magnetization (24). After that, all images were preprocessed using statistical parametric mapping (SPM5, http://www.fil.ion.ucl.ac.uk/spm/). First, the image data underwent

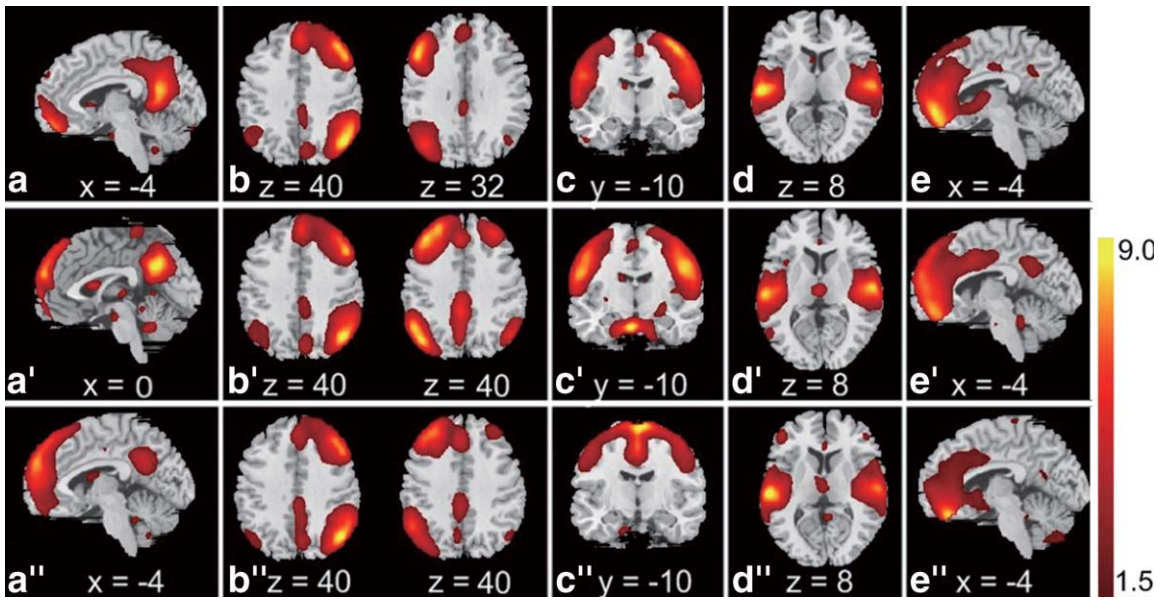

Figure 2. Spatial independent components (brain activation networks) of group results represented with a slice. **a–e**: Default model, memory, motor, auditory, and executive brain networks of resting-state fMRI data. **a′–e′**,**a″–e″**: Five RSNs during poststimulus resting state following acupuncture at GB40 and KI3, respectively. Images are Z statistics overlaid on the average high-resolution scan transformed into standard (MNI152) space. Red to yellow are Z values, ranging from 1.5 to 9.0. The left hemisphere of the brain corresponds to the left side of the axial slice. [Color figure can be viewed in the online issue, which is available at wileyonlinelibrary.com.]

realignment for head motions using least-squares minimization. None of subjects had head movements exceeding 1 mm on any axis and head rotation greater than 1°. A mean image created from the realigned volumes was coregistered with the subject's individual structural T1-weighted volume image. Then the standard MNI template provided by SPM5 was used in spatial normalization with resampling at $2 \times 2 \times 2$ mm. Then these data were filtered by using a band-pass filter (0.01–0.08 Hz) to reduce the effect of low-frequency drift and high-frequency noise (25,26). In the end, the functional images were spatially smoothed with an isotropic Gaussian kernel (full-width at half-maximum [FWHM] = 6 mm).

ICA

We performed a group spatial ICA operation on the smoothed data of all subjects during the 6-minute resting state and the 6-minute post-acupuncture resting epochs of GB40 and KI3 with the fMRI Toolbox (GIFT, http://icatb.sourceforge.net/). The images were reduced to 40 dimensions using principal component analysis, and the number of independent components (ICs) was estimated to be 25 using the MDL criteria (27). The mean ICs of all subjects, the corresponding mean time courses and ICs for each subject were obtained from group ICA separation and back-reconstruction (28). The maps of these ICs across all subjects were generated for a random effect analysis using a one-sample *t*-test ($P < 0.05$, false discovery rate [FDR] corrected). Six ICs were identified as anatomically relevant areas across subjects based on the activation patterns by visual inspection for resting state and post-acupuncture resting states separately (21,22). They comprised five functionally relevant regions involved in DMN, memory (including two ICs, bilateral brain), executive function, auditory processing, and motor function (Fig. 2). The visual-related regions were absent in this study because none of the stimulated acupoints was related to visual function. The intensity values in each spatial map were converted to Z-values to indicate the voxels that contributed most strongly to a particular IC. Voxels with absolute Z-values greater than 1.5 are considered active voxels of the IC in this study (29).

We compared the altered activity patterns of brain regions between resting state and post-acupuncture resting states at GB40 and KI3, respectively. The 12 regions of interest (ROIs), as mentioned in the Introduction, were selected in five functional brain networks (21). The inferior temporal gyrus (Brodmann area [BA] 20/37), anterior cingulate cortex (BA 24/32), and posterior cingulate cortex/precuneus (BA 23/31) are included in the DMN. The superior parietal lobule (BA 7/40), frontopolar area/prefrontal cortex (BA 10/11), and middle temporal gyrus (BA 21) belong to the memory network. The dorsolateral prefrontal cortex (BA 9/46/45) and medial frontal gyrus (BA 11) are located in the executive network. The superior temporal gyrus (BA 41/42) and anterior insula are included in the auditory network. The postcentral gyrus (BA 3) and precentral gyrus (BA 4) belong to the motor network. The spherical ROIs were defined as the sets of voxels included in 6-mm spheres centered on the local maximum activation clusters extracted from ICA. For bilaterally activated regions, we only selected the hemisphere anatomical area with a more significant "Z-score" as the representative ROI (shown in Table 1). Then, the time series were averaged across voxels within each ROI. Finally, the averaged time course across subjects within each

Table 1
Coordinates and Z-scores of the Peak Voxel Within Group ROIs Following Acupuncture at Two Acupoints Compared With the Rest State ($P < 0.05$, FDR-corrected)

	RS						PRSG						PRSK					
		Talairach			Z	V		Talairach			Z	V		Talairach			Z	V
Regions	Hem	x	y	z	Value	Voxels	Hem	x	y	z	Value	Voxels	Hem	x	y	z	Value	Voxels
ITG	R	55	-7	-27	1.68	69	L	-55	-9	-20	2.22	51	L	-55	-11	-21	2.06	46
MeFG	L	-2	50	-18	3.67	38	L	-2	59	21	2.06	34	L	-2	57	21	5.24	39
PCC	R	2	-53	21	4.21	54	R	4	-51	25	1.94	40	L	-2	-51	25	2.13	38
SPL	R	40	-62	49	4.27	64	R	40	-62	49	4.76	64	R	40	-62	49	4.65	64
DLPFC	L	-42	47	-2	4.58	110	R	48	23	38	4.13	44	L	-32	58	3	4.11	51
MTG	L	-44	-63	29	2.20	26	R	50	-63	29	2.18	30	R	48	-63	29	2.59	26
OFC	L	-2	42	-22	1.57	49	L	-2	42	-19	4.78	36	L	-2	38	-20	8.51	54
ACC	L	-2	36	24	2.41	47	L	2	44	-6	4.05	33	L	-2	38	-10	4.93	48
STG	L	-57	-19	8	4.60	43	R	46	-2	-5	4.07	51	L	-59	-21	10	4.27	54
AI	L	-46	-15	10	3.44	67	R	44	-4	-3	3.67	51	L	-49	-23	14	2.85	50
Postcentral	L	-59	-21	14	3.92	53	L	-59	-21	14	3.34	53	L	-59	-21	14	3.81	53
Precentral	R	34	-14	63	3.55	51	R	57	-1	24	3.34	55	L	-8	-18	67	3.30	42

RS, resting state; PRSG, poststimulus resting state at GB40; PRSK, poststimulus resting state at KI3; Hem, hemisphere; ITG, inferior temporal gyrus; MeFG, medial frontal gyrus; PCC, posterior cingulate cortex/precuneus; SPL, superior parietal lobule; DLPFC, dorsolateral prefrontal cortex; MTG, middle temporal gyrus; OFC, frontopolar area/prefrontal cortex; ACC, anterior cingulate cortex; STG, superior temporal gyrus; AI, anterior insula; Postcentral, postcentral gyrus; Precentral, precentral gyrus.

group (resting state and post-acupuncture resting states) was normalized to form a single vector per ROI which then served as the inputs for mGCA.

mGCA

The mGCA has proven effective to investigate the causal networks according to previous neuroimaging studies (30–32). In the current study, we only paid attention to the effective connectivity patterns of the post-acupuncture resting states and the resting state. Let $\mathbf{X}(t) = (x_1(t), x_2(t), \ldots, x_N(t))^T$ be a matrix representing data from the summary time series of the ROIs. Here, $x_i(t)$ $(i = 1, \ldots, N)$ is a time series corresponding to the ith ROI and T denotes matrix transposition. In the following, bold letters represent time domain matrices and capital letters in normal font denote their frequency domain counterparts. The MVAR model of order p is given by:

$$\mathbf{X}(t) - \sum_{n=1}^{p} \mathbf{A}(n)\mathbf{X}(t-n) = \mathbf{E}(t) \quad [1]$$

where $\mathbf{A}(n)$ is the matrix of model parameters consisting of elements $a_{ij}(n)$ and $\mathbf{E}(t)$ is the vector corresponding to the residual error. The order of the autoregressive model was set to 1 using the Schwarz criterion (26,29,30). Then Eq. [1] is transformed to the frequency domain as follows:

$$X(f) = A^{-1}(f)E(f) = H(f)E(f) \quad [2]$$

$$H(f) = A^{-1}(f) \quad [3]$$

where $a_{ij}(f) = \delta_{ij} - \sum_{n=1}^{p} a_{ij}(n)e^{-i2\pi f n}$ and the element a_{ij} corresponds to the matrix A. Here, δ_{ij} is the delta function, expressed as $\delta_{ij} = \begin{cases} 1, & i = j \\ 0, & i \neq j \end{cases}$. Also, $i = 1 \ldots N$, $j = 1 \ldots N$. $H(f)$ is the frequency domain transfer matrix and $h_{ij}(f)$ represents its element in the ith row and jth column. $h_{ij}(f)$ is defined as the nonnormalized DTF corresponding to the influences of ROI j to ROI i (33). The direct DTF (dDTF) is obtained by multiplying $h_{ij}(f)$ with the partial coherence between ROIs i and j. This operation emphasizes the direct causality rather than mediated influences.

To calculate the partial coherence, the cross-spectra are computed as:

$$S(f) = H(f)VH^H(f) \quad [4]$$

Here, V is variance of the matrix $E(f)$ and H in the upper right corner denote conjugate transpose. Then we obtained the partial coherence between ROIs i and j using:

$$\theta_{ij}(f) = \frac{M_{ij}^2(f)}{M_{ii}(f)M_{jj}(f)} \quad [5]$$

where $M_{ij}(f)$ is the cofactor of the matrix S. The partial coherence is confined to the range of [0, 1]. A 0 value here indicates no direct relation between a pair of ROIs in a statistically significant way, while a 1 value indicates there is complete direct association. The dDTF is defined as the sum of all frequency components of the product of the nonnormalized DTF and partial coherence as given in the equation:

$$dDTF_{ij} = \sum_{f} h_{ij}(f)\theta_{ij}(f) \quad [6]$$

Eventually, we obtained the value of dDTF, which only reflects the magnitude of causal influences between the ROIs. To assess the significance of path weights, a null distribution was obtained by generating 2500 sets of surrogate data and calculating the dDTF from these datasets (34). The dDTF value was compared with the null distribution for a one-tailed

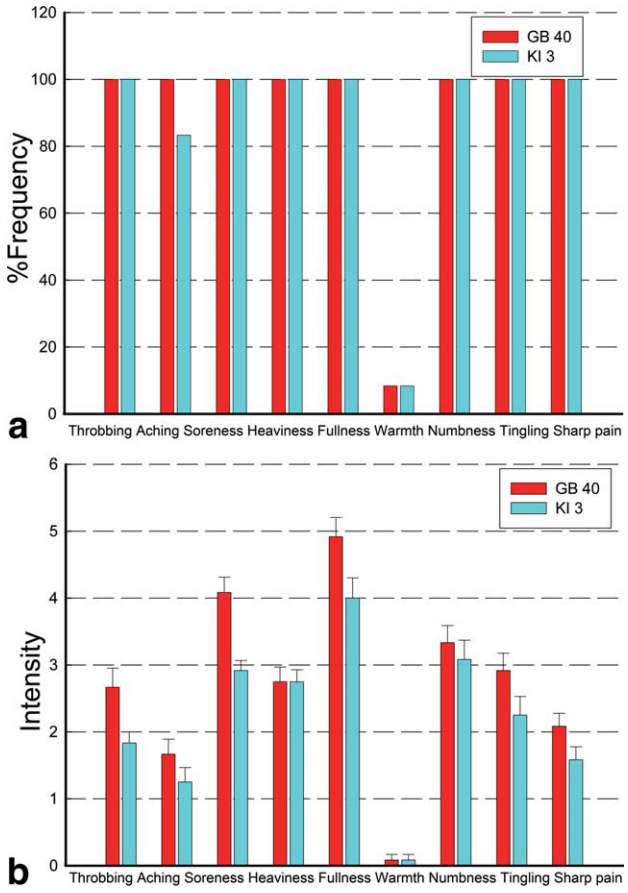

Figure 3. Averaged psychophysical response ($n = 12$). **a**: The percentage of subjects who reported the given sensations (at least one subject experienced the nine sensations listed). The frequency of aching was found greater following acupuncture at GB40. **b**: The intensity of sensations measured by an average score (error bars show 95% confidence intervals) on a scale from 0 denoting no sensation to 10 denoting an unbearable sensation. Significant differences in soreness, fullness, throbbing, tingling, and sharp pain were observed following stimulus at two different acupoints. [Color figure can be viewed in the online issue, which is available at wileyonlinelibrary.com.]

test of significance with a *P*-value of 0.05. The effective connectivity network of the 12 ROIs was constructed by scaling the significant dDTF values. Finally, the measure of In-Out degree was applied to compare the relative information flow in three mGCA networks (26). The In-Out degree of a node is defined as the difference between its number of causal inflows and number of causal out-flows. In-Out degree can identify nodes that differentially affect, or are affected by the other ones.

RESULTS

Psychophysical Results

The prevalence of the sensations (deqi) is expressed as the percentage of individuals in the group that reported the given sensations (Fig. 3a). The intensity is expressed as the average score ± SE (Fig. 3b). No significant differences in the overall frequency of experience were found between acupuncture at GB40 and the control (paired *t*-test, $P > 0.05$). The difference only existed in the aching sensation (GB40: 100%; KI3: 83%). The average stimulus intensities (mean ± SE) were 2.72 ± 0.65 at GB40 and 2.19 ± 0.57 at KI3. We also calculated the Pearson correlation coefficient between the intensity or frequency scores and activity extent of the selected ICs (the percentage of activity voxels). The results of both conditions (GB40 and KI3) indicated that no correlations were observed between individual deqi scores and the activated voxel rate of the ICs.

Effective Connectivity Patterns of the Resting State and Post-Acupuncture Resting State

In this study we explored the causal interactions within and among the resting brain networks modulated by acupuncture at GB40 and KI3. The effective connectivity patterns of brain networks were described as directed graphs. The thickness of connecting lines and the directions of arrows indicate strength and directions of the causal influences (green line in Fig. 4). Only significant effective connectivity ($P < 0.05$) was divided into four levels (25%, 50%, 75%, and 100%) relative to the maximum significant dDTF value and presented in the graphs. The raw mGCA values are also tabulated in Tables 2–4, with significant paths in red color. Significant path weights (on a scale of 0–0.5) were also coded in color matrices and the blue color indicates no significant causality between ROIs from column to row (Fig. 4).

During the resting state, strong causal interactions were observed within the auditory network, between the DMN, executive network, and memory network (shown in Fig. 4a). Following acupuncture at GB40, the superior temporal gyrus (STG) and anterior insula (AI) served as central targets in the network and the central sources were the AI and STG. As shown in Fig. 4b, a bidirectional regulation was forged between the STG and AI, and increased causal influences emerged within the auditory network following acupuncture at GB40. Increased causal relations between the STG and other nodes were also observed, indicating that the interactions between the auditory network and other networks were enhanced following acupuncture stimulation at GB40.

Following acupuncture at KI3, the dorsolateral prefrontal cortex (DLPFC) within the executive network emerged as the central target in the network and the STG was the central source. As shown in Fig. 4c, the reciprocal relation with maximal strength emerged between the STG and the postcentral gyrus. In contrast with Fig. 4b, the number of causal connections incoming into or outgoing from the STG also increased in comparison with that of the resting state. In addition, the causal influences flowing into or outgoing from the middle temporal gyrus (MTG) within the memory network increased. Additionally, the causal influences increased markedly between the executive network and motor network. In order to compare the mGCA networks during resting state, post-acupuncture resting states at GB40 and KI3, we

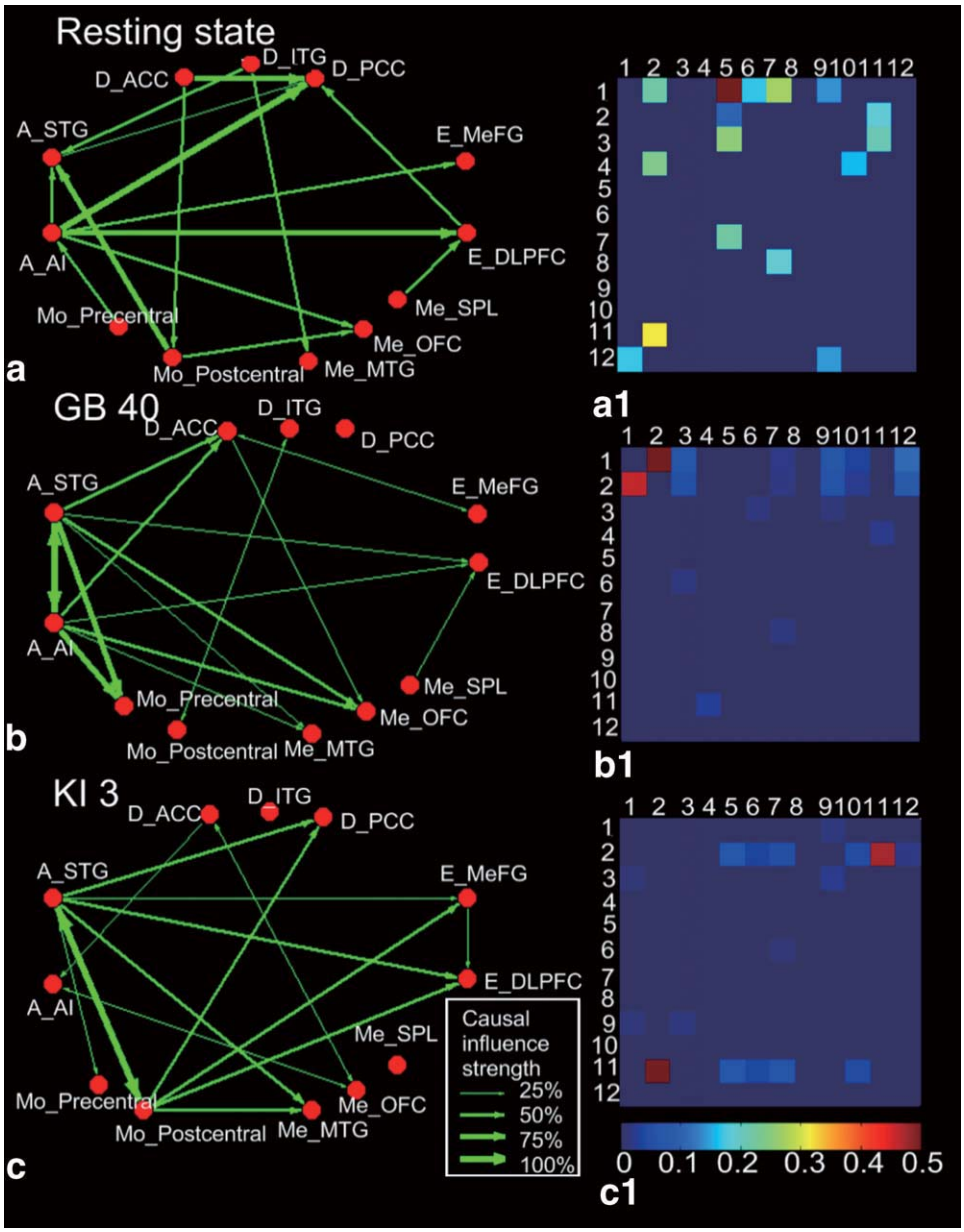

Figure 4. Causal interactions from the mGCA results. The red dots refer to the 12 ROIs. The relative causal influence strength was divided into four levels relative to the maximum significant dDTF value and represented by the thickness of the green line. Significant path weights were also coded in color matrices ($P < 0.05$) and the blue color indicated no significant influences from "column" ROI to "row" ROI. Labels and abbreviations: A_, D_, E_, Me_, and Mo_ represent auditory, default mode, executive, memory, and motor networks, respectively; 1: A_AI (anterior insula); 2: A_STG (superior temporal gyrus); 3: D_ACC (anterior cingulate cortex); 4: D_ITG (inferior temporal gyrus); 5: D_PCC (posterior cingulate cortex); 6: E_MeFG (medial frontal gyrus); 7: E_DLPFC (dorsolateral prefrontal cortex); 8: Me_SPL (superior parietal lobule); 9: Me_OFC (the frontopolar area/prefrontal cortex); 10: Me_MTG (middle temporal gyrus); 11: Mo_Postcentral (postcentral gyrus); 12: Mo_Precentral (precentral gyrus). [Color figure can be viewed in the online issue, which is available at wileyonlinelibrary.com.]

Table 2
Path Weights (Raw mGCA Values) During Resting State and Significant Paths ($P < 0.05$) Are Shown in Italic

	AI	STG	ACC	ITG	PCC	MeFG	DLPFC	SPL	OFC	MTG	Postcentral	Precentral
AI	0.0323	0.0852	0.0054	0.0001	0.0000	0.0000	0.0001	0.0006	0.0011	0.0050	0.0175	*0.0858*
STG	*0.1479*	0.0020	0.0039	*0.1712*	0.0003	0.0001	0.0006	0.0512	0.0000	0.0040	*0.2676*	0.0005
ACC	0.0007	0.0409	0.0838	0.0092	0.0000	0.0013	0.0000	0.0025	0.0423	0.0116	0.0300	0.0027
ITG	0.0000	0.0033	0.0047	0.1857	0.0000	0.0029	0.0001	0.0007	0.0051	0.0849	0.0380	0.0002
PCC	*0.4865*	*0.0067*	*0.1910*	0.0000	0.0236	0.0001	*0.1487*	0.0039	0.0005	0.0423	0.0001	0.0003
MeFG	*0.0822*	0.0019	0.0016	0.0064	0.0000	0.0678	0.0000	0.0001	0.0566	0.0013	0.0008	0.0002
DLPFC	*0.2090*	0.0116	0.0001	0.0028	0.0000	0.0020	0.0242	*0.1109*	0.0002	0.0025	0.0160	0.0001
SPL	0.0002	0.0020	0.0039	0.0019	0.0003	0.0001	0.0006	0.0512	0.0000	0.0040	0.0017	0.0005
OFC	*0.0506*	0.0152	0.0429	0.0097	0.0000	0.0475	0.0000	0.0000	0.1251	0.0004	*0.0557*	0.0005
MTG	0.0004	0.0022	0.0066	*0.0743*	0.0008	0.0006	0.0001	0.0015	0.0002	0.2123	0.0021	0.0044
Postcentral	0.0004	*0.1056*	*0.1344*	0.0113	0.0000	0.0001	0.0000	0.0002	0.0019	0.0006	0.6867	0.0005
Precentral	0.0000	0.0004	0.0050	0.0007	0.0000	0.0004	0.0000	0.0006	0.0009	0.0142	0.0054	0.0803

AI, anterior insula; STG, superior temporal gyrus; ACC, anterior cingulate cortex; ITG, inferior temporal gyrus; PCC, posterior cingulate cortex; MeFG, medial frontal gyrus; DLPFC, dorsolateral prefrontal cortex; SPL, superior parietal lobule; OFC, frontopolar area/prefrontal cortex; MTG, middle temporal gyrus; Postcentral, postcentral gyrus; Precentral, precentral gyrus.

Table 3
Path Weights (Raw mGCA values) During Poststimulus Resting State at GB40 and Significant Paths ($P < 0.05$) Are Shown in Italic

	AI	STG	ACC	ITG	PCC	MeFG	DLPFC	SPL	OFC	MTG	Postcentral	Precentral
AI	0.2848	*0.2486*	0.0024	0.0000	0.0000	0.0000	0.0002	0.0000	0.0017	0.0013	0.0007	0.0009
STG	*0.2699*	0.2456	0.0022	0.0000	0.0001	0.0000	0.0002	0.0000	0.0018	0.0011	0.0016	0.0008
ACC	*0.0318*	*0.0268*	0.0104	0.0000	0.0005	*0.0080*	0.0000	0.0002	0.0052	0.0002	0.0032	0.0005
ITG	0.0000	0.0002	0.0000	0.0629	0.0007	0.0003	0.0005	0.0005	0.0000	0.0020	*0.0143*	0.0006
PCC	0.0007	0.0022	0.0008	0.0024	0.0057	0.0000	0.0004	0.0023	0.0001	0.0014	0.0000	0.0000
MeFG	0.0001	0.0007	*0.0081*	0.0008	0.0000	0.0090	0.0002	0.0007	0.0003	0.0003	0.0026	0.0000
DLPFC	*0.0096*	*0.0088*	0.0000	0.0041	0.0010	0.0008	0.0030	*0.0075*	0.0000	0.0021	0.0075	0.0000
SPL	0.0005	0.0004	0.0003	0.0014	0.0018	0.0007	0.0022	0.0276	0.0000	0.0007	0.0008	0.0000
OFC	*0.0311*	*0.0305*	*0.0073*	0.0001	0.0001	0.0004	0.0000	0.0000	0.0239	0.0000	0.0004	0.0000
MTG	*0.0160*	*0.0121*	0.0002	0.0044	0.0009	0.0003	0.0006	0.0006	0.0000	0.0315	0.0015	0.0002
Postcentral	0.0028	0.0059	0.0009	*0.0107*	0.0000	0.0007	0.0005	0.0002	0.0001	0.0005	0.0642	0.0000
Precentral	*0.0585*	*0.0427*	0.0026	0.0074	0.0001	0.0001	0.0000	0.0000	0.0003	0.0012	0.0003	0.0040

Abbreviations as in Table 2.

sorted In-Out degrees of three effective connectivity networks in a descending order as shown in Fig. 5.

DISCUSSION

In the current study we found that different causal influences within and among the RSNs can be modulated by acupuncture at GB40, compared with KI3 as a control condition (belonging to the same nerve segment but different meridians). Our results were consistent with previous findings and provided further evidence to support that acupuncture can exert sustained modulatory effects on the poststimulus resting brain networks (14,16,17,19). More important, we also demonstrated that acupuncture at different acupoints may exert heterogeneous modulatory effects on the causal interactions of brain networks during the poststimulus resting period. Following stimulation at GB40, the STG and AI within the auditory network displayed remarkably increased causal influences in comparison with that of the resting state. As for the control acupoint KI3, no remarkable changes within the auditory network were observed. By comparing the causal brain networks of the resting state and post-acupuncture resting states, we found that acupuncture could exert different modulatory effects on RSNs at functionally irrelevant acupoints.

The exploration of resting-state brain networks has recently gained popularity (19,21,29), and some researchers focused on the modulatory effects of acupuncture on RSNs, mainly using functional connectivity analysis (17,19). This method primarily focused on correlated patterns between a seed region and other brain structures involved in certain functions throughout the brain. However, it might not directly characterize causal interactions among multiple brain regions. Alternatively, the Granger causality analysis may be an appropriate approach to study the directional interactions within and among the RSNs. However, a pairwise Granger causality framework does not take into account the influences of a third brain region and cannot discern the direct or indirect causal connectivity (35). Hence, we introduced mGCA to detect the direct causal relations among multiple brain areas and discern both the direction and strength of information flow within and among brain networks.

In agreement with the previous study, our ICA results of the consistent networks included DMN, memory network, executive network, auditory network, and motor network (21). In addition, the present study suggested that the frontopolar area/

Table 4
Path Weights (Raw mGCA Values) During Poststimulus Resting State at KI3 and Significant Paths ($P < 0.05$) Are Shown in Italic

	AI	STG	ACC	ITG	PCC	MeFG	DLPFC	SPL	OFC	MTG	Postcentral	Precentral
AI	0.0327	0.0058	*0.0067*	0.0006	0.0004	0.0004	0.0000	0.0002	*0.0077*	0.0011	0.0000	0.0006
STG	0.0006	0.2963	0.0000	0.0000	0.0032	0.0018	0.0026	0.0000	0.0000	0.0012	*0.2988*	0.0009
ACC	0.0059	0.0003	0.0235	0.0000	0.0001	0.0004	0.0000	0.0000	*0.0088*	0.0004	0.0000	0.0000
ITG	0.0039	0.0031	0.0005	0.0011	0.0001	0.0030	0.0022	0.0010	0.0030	0.0025	0.0005	0.0050
PCC	0.0005	*0.0406*	0.0001	0.0000	0.0175	0.0002	0.0007	0.0003	0.0000	0.0039	*0.0411*	0.0003
MeFG	0.0005	*0.0191*	0.0005	0.0004	0.0001	0.0218	0.0060	0.0000	0.0016	0.0000	*0.0229*	0.0014
DLPFC	0.0000	*0.0285*	0.0000	0.0003	0.0006	*0.0064*	0.0316	0.0028	0.0004	0.0007	*0.0346*	0.0015
SPL	0.0003	0.0003	0.0000	0.0003	0.0005	0.0001	0.0056	0.0083	0.0020	0.0020	0.0001	0.0022
OFC	*0.0093*	0.0007	*0.0134*	0.0004	0.0000	0.0023	0.0006	0.0013	0.0256	0.0002	0.0000	0.0002
MTG	0.0022	*0.0253*	0.0008	0.0009	0.0066	0.0000	0.0016	0.0020	0.0003	0.0188	*0.0246*	0.0007
Postcentral	0.0000	*0.2830*	0.0000	0.0000	0.0031	0.0020	0.0029	0.0000	0.0000	0.0011	0.3019	0.0003
Precentral	0.0006	*0.0111*	0.0000	0.0006	0.0002	0.0016	0.0015	0.0012	0.0001	0.0004	0.0041	0.0298

Abbreviations as in Table 2.

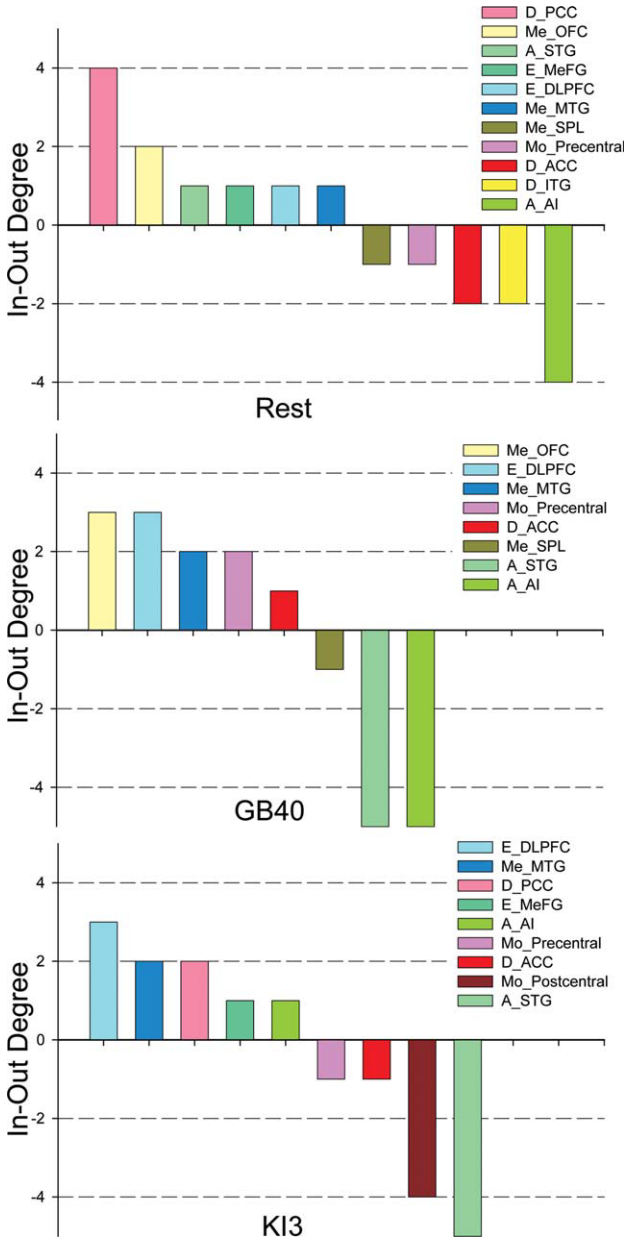

Figure 5. The In-Out degrees of each node in three mGCA networks were ranking in descending order. A node with a highly positive In-Out degree can be considered to be largely affected by other nodes. On the contrary, a node with negative causal flow exerts a strong causal influence on other ones. Only the brain regions with a nonzero value of In-Out degree are listed. Labels and abbreviations as in Fig. 4. [Color figure can be viewed in the online issue, which is available at wileyonlinelibrary.com.]

prefrontal cortex (OFC) and posterior cingulate cortex/precuneus (PCC) served as central targets in the network following acupuncture at GB40, and the central sources were the AI and STG (Fig. 5). Enhanced interactions emerged within the auditory network, and also existed between it and other networks since GB40 is an audition-related acupoint (37). Following acupuncture at KI3, we identified that the DLPFC emerged as the central target in the causal network and the STG was the central source. Lee et al (38) pointed out that acupuncture at KI3 could improve mood and cognitive functions of patients with Alzheimer's disease. The DLPFC is exactly located in the frontal lobe and associated with cognitive and executive function (39). In contrast to the resting state, the causal influences between the auditory network and others were unchanged, but between the executive network and others were enhanced, suggesting that the cognitive level grew higher following acupuncture at KI3 because the frontal lobe is an important region among cognitive brain areas (40). The PCC, as one of the cognitive-related vital nuclei (36), had two causal inflows coming into it following acupuncture at KI3, but no causal connection was found following acupuncture at GB40. These different effective connectivity patterns of post-acupuncture resting state may be related to the special effects of acupuncture in clinical settings. The above results likely validate the relatively functional specificity of different acupoints.

A recent fMRI study on DMN demonstrated that a causal target in the neuronal activity propagation process tends to have a stronger BOLD activity, suggesting that causal influences may predict the neuronal activity levels (26). This article also indicated that the power spectral intensity of the mean time series extracted from a brain region is in direct proportion to causal inflows of the brain region. Since strength is a reflection of the energy flow (26), we speculated that the strength of neural activity would be stronger if the sum of causal inflows with weight was larger within and among multiple RSNs. A strictly quantitative measure will be a further task. The acupoints KI3 and GB40 may share some common features of the BOLD response following acupuncture because they belong to the same nerve segment. Our results indicated that AI and STG both had stronger strength in the network following acupuncture at GB40. As for KI3, the regions with stronger strength were the postcentral gyrus and STG. Therefore, the postcentral gyrus, AI, and STG may show sustained activation during post-acupuncture resting states. This speculation was consistent with the investigation that the insular cortex and sensorimotor areas consistently give positive responses after acupuncture stimulation, regardless of acupoint locations or manipulation modes (8,9). Furthermore, decreased neural activity within DMN was observed following acupuncture manipulations (17). In our results, decreased connectivity emerged in the PCC within DMN following acupuncture at GB40 in comparison with the ITG within DMN following acupuncture at KI3 in the network, and both nuclei are probably regions of deactivation.

In conclusion, the current study demonstrated that acupuncture at different acupoints could exert different causal influences within and among the RSNs and these effects can last a long period after the needling process is terminated. We propose that acupuncture as an external intervention may regulate the RSNs dissimilarly across different acupoints. These preliminary investigations are expected to provide a new clue for deciphering the relatively function-oriented specificity of acupuncture effects. Our findings may help to understand the neurophysiological mechanisms underlying acupuncture specificity.

REFERENCES

1. National Institutes of Health. NIH consensus conference statement acupuncture. JAMA 1998;280:1518–1524.
2. Li G, Cheung R, Ma Q, Yang E. Visual cortical activations on fMRI upon stimulation of the vision-implicated acupoints. Neuroreport 2003;14:669–673.
3. Lee H, Park H, Kim S, et al. Acupuncture stimulation of the vision-related acupoint (BL-67) increases c-Fos expression in the visual cortex of binocularly deprived rat pups. Am J Chinese Med 2002;2:379–385.
4. Kong J, Kaptchuk T, Webb J, et al. Functional neuroanatomical investigation of vision-related acupuncture point specificity—a multisession fMRI study. Human Brain Mapp 2009;30:38–46.
5. Wesolowski T, Lotze M, Domin M, et al. Acupuncture reveals no specific effect on primary auditory cortex: a functional magnetic resonance imaging study. Neuroreport 2009;20:116–120.
6. Fang J, Jin Z, Wang Y, et al. The salient characteristics of the central effects of acupuncture needling: limbic-paralimbic-neocortical network modulation. Hum Brain Mapp 2009;30: 1196–1206.
7. Hui K, Liu J, Makris N, et al. Acupuncture modulates the limbic system and subcortical gray structures of the human brain: evidence from fMRI studies in normal subjects. Hum Brain Mapp 2000;9:13–25.
8. Hui K, Liu J, Marina O, et al. The integrated response of the human cerebro-cerebellar and limbic systems to acupuncture stimulation at ST 36 as evidenced by fMRI. Neuroimage 2005;27: 479–496.
9. Bai L, Qin W, Tian J, et al. Time-varied characteristics of acupuncture effects in fMRI studies. Hum Brain Mapp 2009;30: 3445–3460.
10. Mayer D.J. Acupuncture: an evidence-based review of the clinical literature. Anal Rev Med 2000;51:49–63.
11. Beijing S. Nanjing Colleges of Traditional Chinese Medicine. Essentials of Chinese zcupuncture. Beijing: Foreign Language Press; 1980.
12. Price D, Rafii A, Watkins L, Buckingham B. A psychophysical analysis of acupuncture analgesia. Pain 1984;19:27–42.
13. Bai L, Tian J, Zhong C, et al. Acupuncture modulates temporal neural responses in wide brain networks: evidence from fMRI study. Mol Pain 2010;6:73.
14. Bai L, Qin W, Tian J, Dai J, Yang W. Detection of dynamic brain networks modulated by acupuncture using a graph theory model. Prog Nat Sci 2009;19:827–835.
15. Bai L, Yan H, Li L, et al. Neural specificity of acupuncture stimulation at pericardium 6: evidence from an FMRI study. J Magn Reson Imaging 2010;31:71–77.
16. Bai L, Qin W, Liang J, Tian J, Liu Y. Spatiotemporal modulation of central neural pathway underlying acupuncture action: a systematic review. Curr Med Imaging Rev 2009;5:167–173.
17. Dhond R, Yeh C, Park K, Kettner N, Napadow V. Acupuncture modulates resting state connectivity in default and sensorimotor brain networks. Pain 2008;136:407–418.
18. Liu J, Qin W, Guo Q, et al. Distinct brain networks for time-varied characteristics of acupuncture. Neurosci Lett 2010;468: 353–358.
19. Bai L, Qin W, Tian J, et al. Acupuncture modulates spontaneous activities in the anticorrelated resting brain networks. Brain Res 2009;1279:37–49.
20. McKeown M, Jung T, Makeig S, et al. Spatially independent activity patterns in functional MRI data during the Stroop color-naming task. Proc Natl Acad Sci U S A 1998;95:803–810.
21. Damoiseaux J, Rombouts S, Barkhof F, et al. Consistent resting-state networks across healthy subjects. Proc Natl Acad Sci U S A 2006;103:13848–13853.
22. Demirci O, Stevens M, Andreasen N, et al. Investigation of relationships between fMRI brain networks in the spectral domain using ICA and Granger causality reveals distinct differences between schizophrenia patients and healthy controls. Neuroimage 2009;46:419–431.
23. Liao W, Ding J, Marinazzo D, et al. Small-world directed networks in the human brain: multivariate Granger causality analysis of resting-state fMRI. Neuroimage 2011;54:2683–2694.
24. Castelli F, Glaser D, Butterworth B. Discrete and analogue quantity processing in the parietal lobe: a functional MRI study. Proc Natl Acad Sci U S A 2006;103:4693–4698
25. Greicius M, Krasnow B, Reiss A, Menon V. Functional connectivity in the resting brain: a network analysis of the default mode hypothesis. Proc Natl Acad Sci U S A 2003;100:253–258.
26. Jiao Q, Lu G, Zhang Z, et al. Granger causal influence predicts BOLD activity levels in the default mode network. Hum Brain Mapp 2011;32:154–161.
27. Li Y, Adali T, Calhoun V. Sample dependence correction for order selection in fMRI analysis. In: Proc ISBI; 2006. p 1072–1075.
28. Calhoun V, Adali T, Pearlson G, Pekar J. A method for making group inferences from functional MRI data using independent component analysis. Hum Brain Mapp 2001;14:140–151.
29. Liao W, Mantini D, Zhang Z, et al. Evaluating the effective connectivity of resting state networks using conditional Granger causality. Biol Cybern 2010;102:57–69.
30. Deshpande G, LaConte S, James G, Peltier S, Hu X. Multivariate Granger causality analysis of fMRI data. Hum Brain Mapp 2009; 30:1361–1373.
31. Kamiński M, Ding M, Truccolo W, Bressler S. Evaluating causal relations in neural systems: Granger causality, directed transfer function and statistical assessment of significance. Biol Cybern 2001;85:145–157.
32. Roebroeck A, Formisano E, Goebel R. Mapping directed influence over the brain using Granger causality and fMRI. Neuroimage 2005;25:230–242.
33. Kus R, Kaminski M, Blinowska K. Determination of EEG activity propagation: pair-wise versus multichannel estimate. IEEE Trans Biomed Eng 2004;51:1501–1510.
34. Theiler J, Eubank S, Longtin A, Galdrikian B, Doyne Farmer J. Testing for nonlinearity in time series: the method of surrogate data. Physica D 1992;58:77–94.
35. Granger C. Investigating causal relations by econometric models and cross-spectral methods. Econometrica 1969;424–438.
36. Sridharan D, Levitin D, Menon V. A critical role for the right fronto-insular cortex in switching between central-executive and default-mode networks. Proc Natl Acad Sci U S A 2008;105: 12569–12574.
37. MacPherson H, Thorpe L, Thomas K, Campbell M. Acupuncture for low back pain: traditional diagnosis and treatment of 148 patients in a clinical trial. Complement Ther Med 2004;12: 38–44.
38. Lee M, Shin B, Ernst E. Acupuncture for Alzheimer's disease: a systematic review. Int J Clin Pract 2009;63:874–879.
39. Elsa B, Philip A, Kevin P, Rosalie J. On age differences in prefrontal function: the importance of emotional/previous cognitive integration. Neuropsychologia 2010;48:319–333.
40. Liu B, Song M, Li J, et al. Prefrontal-related functional connectivities within the default network are modulated by COMT val158-met in healthy young adults. J Neurosci 2010;30:64–69.